Operation of the Electron Cyclotron system in the ITER new baseline

Mireille Schneider[1*], *Mélanie* Preynas[1], *Jörg* Stober[2], *Natalia* Casal[1], *Maksim* Dubrov[1], *Lorenzo* Figini[3], *Yuri* Gribov[1], *Emanuele* Poli[2], and *Peter* de Vries[1]

[1]ITER Organization, Route de Vinon-sur-Verdon, CS 90 046, 13067 St. Paul-lez-Durance, France
[2]Max-Planck-Institut für Plasmaphysik, Garching, Germany
[3]Istituto per la Scienza e Tecnologia dei Plasmi, CNR, 20125 Milano, Italy

Abstract. The ITER Research Plan (IRP) has undergone significant modifications based on the change of First Wall (FW) material from beryllium (Be) to tungsten (W). Such a change, together with the constraint of achieving Q=10 for 300s with a neutron fluence of ~1% of the total ITER lifetime fluence, calls for a modification of the heating mix, now dominated by Electron Cyclotron Heating (ECH), to ensure robust plasma operation and provide the most flexible operational space, w.r.t. to Ion Cyclotron Heating (ICH) and Neutral Beam Injection (NBI). This contribution gives first a brief overview of the revised heating mix in the new ITER baseline, with a description of the planned new configuration of the EC system, i.e. the set of Upper and Equatorial launchers needed to inject up to 60-67 MW to ITER plasmas. Delivery of this increased power requires the installation of a second equatorial launcher for the DT phase. The various contexts for which the EC system will be applied cover plasma initiation, wall conditioning, heating, current drive, W and MHD control, to achieve high-performance plasmas and ensure the completion of ITER milestones for the various phases of the IRP. The operational strategy for each phase will be described, in terms of optimal choice of launchers, applied power and polarization, taking into account the plasma evolution during a discharge. The operational conditions are adjusted to achieve the best plasma performance while ensuring that stray radiation does not damage in-vessel components.

1 Introduction

A key component of the new ITER baseline and associated Research Plan (IRP) is the change of first wall (FW) material from beryllium (Be) to tungsten (W) [1]. This very significant change requires a modified Heating and Current Drive (H&CD) strategy; the overall H&CD power is substantially increased to reduce the need for fusion alpha power in the development path towards Q=10 in DT-1 operation, which must be achieved in the first DT campaign (DT-1) of the new baseline within a neutron fluence (3.5×10^{25}) limited to 1% of the total ITER lifetime neutron budget [1]. Emphasis is placed on Electron Cyclotron Heating (ECH), the power of which is increased by a factor 2 to 3 with respect to the 2016 baseline, to overcome potential increases in the core radiation which might be experienced due to the increased W source. The Ion Cyclotron Heating (ICH) power is reduced to 10 MW, with a possible upgrade to 20 MW in DT-1. The new baseline is split into three distinct operational phases:

- Start of Research Operation (SRO), with 40 MW ECH, 10 MW ICH and no NBI. The main goals of this phase are to demonstrate H-mode operation up to 7.5 MA / 2.65 T in deuterium and L-mode operation at full magnetic energy, i.e. 15 MA / 5.3T in hydrogen.
- DT-1: ECH will be upgraded to 60-67 MW (depending on whether 3 or 4 upper launchers are operated, as described later in the paper). ICH will be upgraded to 20 MW if it demonstrates no detrimental increase of the core W concentration. The Neutral Beam Injection (NBI) system will operate with a total available power of 33 MW. The main goal of DT-1 is to demonstrate Q=10 in inductive operation, for a duration of ~300-500s.
- DT-2 aims to demonstrate routine hybrid and steady-state operation. For this phase, the NBI system may be upgraded to 49.5 MW to increase the source of non-inductive current drive to achieve high plasma current (typically ~10 MA) in non-inductive operation.

The new baseline relies heavily on the EC system, essential for successful high performance plasma operation, by providing the following functionalities:

- EC-assisted plasma breakdown and burn-through for robust plasma operation. ECH helps to ionize the prefill gas, accelerating electrons by means of the ECH wave electric field rather than only using the toroidal electric field generated by the tokamak magnets (which is low in a superconducting device). It also increases the plasma temperature during the

* Corresponding author: mireille.schneider@iter.org

burn-through phase to overcome ionisation and radiation losses while the plasma pressure increases.

- ECH during the plasma current ramp-up will mitigate W radiative collapse by expelling W from the core; by heating the plasma it also reduces the magnetic flux consumption such that longer current plateaux can be achieved.
- The ECH system provides a significant source of Electron Cyclotron Current Drive (ECCD) which is the second main source of external non-inductive current drive (after NBI). ECCD is also used for current profile shaping to achieve high plasma performance necessary for non-inductive operation in DT-2.
- ECH, like other H&CD sources, is required for H-mode access by increasing the power crossing through the separatrix to above the L-H power threshold. In the SRO phase, it will be the dominant heating source for H-mode access and this is in fact one of the main drivers with a power increase to 40 MW compared with only 20 MW in the non-active phases of the 2016 baseline. It also helps to achieve the necessary temperature to reach high fusion gain in the DT phases.
- ECH/ECCD is used for MHD control (sawteeth, NTMs, Alfvén eigenmodes)
- Finally, the ECH system may also be deployed for Electron Cyclotron Wall Conditioning (ECWC) [2], principally as a means to remove adsorbed impurities from the main chamber walls (as opposed to Ion Cyclotron Wall Conditioning (ICWC) which is primarily a vehicle for isotope exchange (hence fuel retention control).

2 Operational conditions of the ITER EC system

The ITER EC system consists of a set of equatorial (EL) and upper (UL) launchers as displayed in Fig. 1.

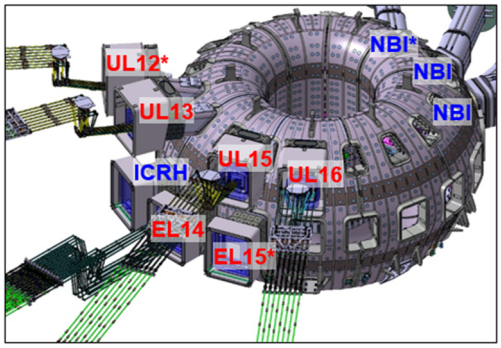

Fig. 1. Set of ITER EC launchers (in red), together with the ICH antenna and 2 to 3 NBI injectors (in blue). Asterisks denote possible system upgrades.

Each EL consists of three mirrors: top (TSM), middle (MSM) and bottom (BSM), with each directing 8 beams into the chamber. The ULs consist of 2 steering mirrors: upper (USM) and lower (LSM), each directing 4 beams. All mirrors inject in the co-current direction except the TSM of the 1st EL (the launcher in Equatorial Port 14, referred as EL14 in Fig. 1). Each beam is connected to a 1 MW gyrotron and is considered to inject about 0.83 MW into the plasma (due to losses along the transmission lines and in the launchers). For SRO, only 3 ULs and 1 EL will be installed. From DT-1 onwards, 2 ELs and 3 to 4 ULs will be installed depending on the outcome of the SRO campaign. All launchers are steerable in one direction (defined as γ steering angle), mostly in the poloidal direction, with a small variation of the toroidal angle (few degrees). An exception is made for the 2nd EL to be installed in Equatorial Port 15 (referred to henceforth as EL15) from DT-1, which will have no steering capabilities, hence special care has been taken to choose the appropriate toroidal and poloidal direction of its mirrors as described in Section 3. The poloidal steering range of the 1st EL and the ULs is illustrated in Fig. 2. The poloidal and toroidal angles are named α and β respectively. A normalised poloidal steering γ_N is also defined such that $\gamma_N = -1$ and 1 correspond respectively to the most upwards and most downwards directions in the poloidal plane.

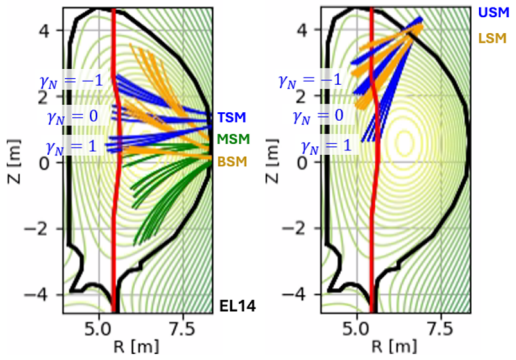

Fig. 2. Poloidal steering range for the three mirrors of EL14 (left figure) and the two mirrors of the ULs (right figure).

As discussed later in the paper, the optimal radial coverage of the 2nd EL has been decided to be within the radial range or normalised toroidal flux coordinate ρ ~ [0.2,0.4]. On a general basis, the ELs focus on the core while the ULs are designed to inject off-axis with a very narrow deposition to afford efficient Neoclassical Tearing Mode (NTM) control capabilities. The available EC power for each radial location in the plasma is given in Table 1 for the various phases of ITER operation. It accounts for the individual accessibility of each mirror of the launchers.

Table 1. Maximum EC power for each radial location. Core values differ between SRO and DT due to the additional EL. Values with asterisk assume upgrade from 3 to 4 ULs.

ρ ~ [0,0.2]	ρ ~ [0.2,0.4]	ρ ~ [0.4,0.6]	ρ ~ [0.6,0.8]
20 MW	20 MW (SRO) 40 MW (DT)	23.3 MW 26.7 MW*	10 MW 13.3 MW*
ρ ~ [0,0.4]		ρ ~ [0.4,0.8]	
20 MW (SRO) 40 MW (DT)		33.3 MW 40 MW*	
Total: ρ ~ [0,1]			
60 MW 66.7 MW*			

To choose the optimal operational conditions of the EC system in the various phases of the IRP, three constraints must be taken into account:

- The magnetic field, which imposes the radial location of the resonance layer. Given that core heating is even more essential with the W first wall to reduce the W core concentration, the new baseline now focuses exclusively on operating at 2.65 T (half-field, 2nd harmonic absorption) and 5.3 T (full-field, fundamental absorption).

- The local plasma pressure which may affect the overall absorption efficiency of the wave if it becomes too low.

- The local plasma density which limits the propagation of X-mode polarized waves, due to the so-called Right Hand density cut-off.

Owing to its higher absorption in comparison with O-mode polarization, ECH will be injected as much as possible with X-mode polarization. However, as shown in the Clemmow–Mullaly–Allis (CMA) diagram of Fig. 3, X-mode is not always appropriate due to the wave propagation properties. The electron cyclotron frequency ω_{ce} and the Right-Hand (RH) cut-off frequency ω_R are defined as:

$$\omega_{ce} = \frac{eB}{m_e} \ ,$$

$$\omega_R \approx \sqrt{\left(\frac{eB}{2m_e}\right)^2 + \frac{n_e e^2}{\varepsilon_0 m_e}} + \frac{eB}{2m_e} \ ,$$

where B is the magnetic field, m_e the electron mass, n_e the electron density, e the elementary charge and ε_0 the vacuum permittivity.

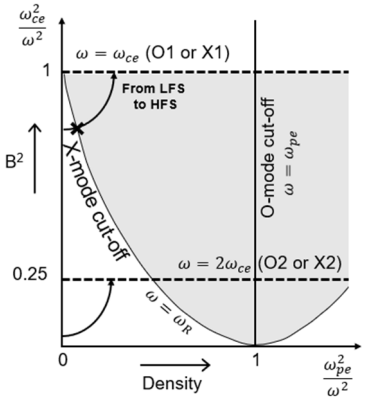

Fig. 3. CMA diagram for ECH propagation properties; $\boldsymbol{\omega_{ce}}$ and $\boldsymbol{\omega_{pe}}$ represent the electron cyclotron and plasma frequencies respectively; $\boldsymbol{\omega}$ is the wave frequency and $\boldsymbol{\omega_R}$ the cut-off frequency.

Detailed explanations of such a diagram can be found e.g. in [3]. For ITER, it gives the following indication:

- O-mode waves can propagate for any plasma density in the ITER operational density range, both at 2.65T (O2) and 5.3T (O1).

- X-mode waves can propagate for any density at 2.65 T (X2) but not at 5.3 T (X1) where the RH cut-off may be encountered. At very low density, the X1 cut-off layer can be very close to the resonance layer (at zero density, the two are superimposed, as can be seen from the equations above), in which case some absorption would still occur. In contrast, at high density, the cut-off layer is at the separatrix, hence no absorption can take place.

Another operational constraint specific to ITER is ECH at 2.65 T (X2) for which the 3rd harmonic resonance (X3) is inside the plasma at the very edge. Under such conditions, for H-mode operation when the edge plasma density and temperature are high due to the pedestal (see the kinetic profiles for an H-mode half-field scenario in Fig. 4), the quasi totality of the EC power is absorbed at the edge, preventing ECH core heating, as shown in Fig. 5. In L-mode, the X3 edge absorption is negligible due to the low edge plasma density and temperature, in which case X2 is more appropriate. This means that the polarization of the wave should be adjusted according to the confinement regime, implying a change of polarization during an L-H transition when operating at 2.65 T.

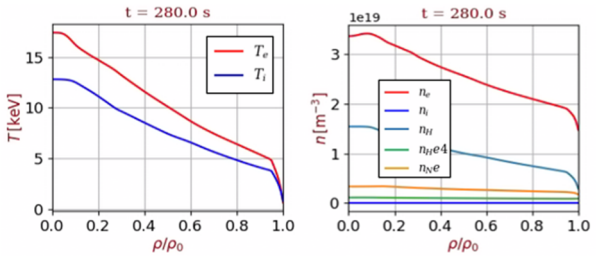

Fig. 4. Temperature (left) and density (right) profiles for the JINTRAC 2.65 T / 7.5 MA H-mode 104104/33 IMAS scenario

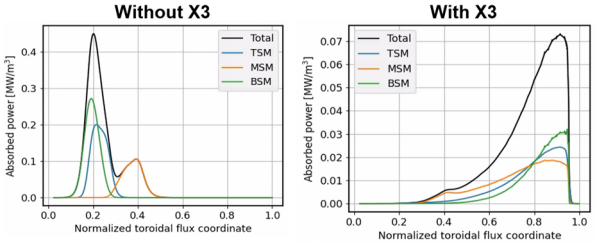

Fig. 5. ECH deposition profiles obtained with the kinetic profiles from Fig. 4, without (left) and with (right) the 3rd harmonic taken into account.

To summarise, the appropriate wave polarization for each operational condition is the following:

- At 5.3 T: O1, due to the density cut-off at X1. Note that a few percent of each beam launched in the plasma is expected to be in the wrong polarization (i.e. cross-polarization X1), leading to extra EC power losses, as discussed in Section 4. The choice of O1 can be questioned in the plasma current ramp-up, for which the plasma pressure is low, hence the O-mode absorption efficiency is significantly reduced. It is precisely in this phase of the discharge that the density can be low enough for the X1 cut-off to be close to the resonance, leading to significant absorption of X1 wave. A detailed analysis of the dynamics of the EC absorption in the current ramp-

up would be required to further assess the optimal wave polarization while the plasma current rises.

- At 2.65 T: X2, due to its better efficiency than O2 at low plasma pressure, except in H-mode when the polarization should be switched to O2 due to the X3 parasitic absorption. Such polarization transitions can be instantaneously handled provided that not all gyrotrons are used simultaneously in which case those which are turned off are already prepared with the alternative polarization. Otherwise, the change of polarization for a beamline during gyrotron operation would need about 3 seconds.

3 Preliminary design of the 2nd EL

3.1 Modelling tools and environment

ECH/ECCD modelling for the key scenarios of the IRP is required to find the optimal angles of the 2nd EL, which will have no steering capability. This modelling has been performed with the TORBEAM beam-tracing code [4], describing the propagation and absorption of EC waves in the plasma, within the ITER Integrated Modelling and Analysis Suite (IMAS) [5], which offers a standard for both experimental and simulated data. Three cases have been picked from the IMAS scenario database, to cover the main variations of EC operational conditions:

- The 15 MA / 5.3 T DT baseline H-mode scenario: this is given priority since the best ECH/ECCD performance must be achieved for this scenario (IMAS DINA-JINTRAC 134173/106) → O1 absorption.
- An L-mode 7.5 MA / 2.65 T scenario (IMAS 105078/6) → X2 absorption.
- An H-mode 7.5 MA / 2.65 T scenario (IMAS 105045/1) → O2 absorption.

Simulations are made without self-consistency between the magnetic equilibrium, kinetic profiles and ECH/ECCD calculations. However, since the original scenarios already contain ECH/ECCD, this approach can be considered as a good approximation provided that the same EC power waveforms are used in the input scenario and in the standalone ECH/ECCD modelling. For self-consistent modelling between transport and ECH/ECCD, TORBEAM can, for example, be used within the H&CD workflow [6] now integrated in JINTRAC [7] as part of the High-Fidelity Plasma Simulator (HFPS). An example of using the H&CD workflow inside the HFPS can be found e.g. in [8].

The IMAS TORBEAM coupling is illustrated in Fig. 6. It takes the input `equilibrium` and `core_profiles` Interface Data Structures (IDS) from an existing scenario (read from the scenario database) or from a transport suite, when used self-consistently in a transport solver; it takes the input `ec_launchers` IDS from the Machine Description database which is dynamically filled with the desired EC waveforms. As an output, it fills the `waves` IDS which is either stored on disk (standalone TORBEAM calculation) or transferred to the rest of the workflow (for the usage within a transport suite).

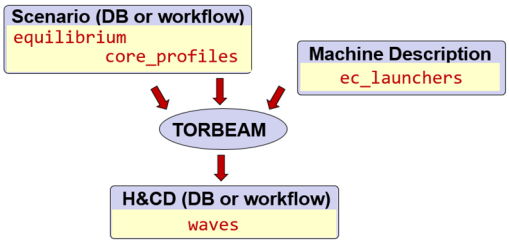

Fig. 6. IMAS interface of the TORBEAM code, which can be used standalone or within the H&CD workflow.

3.2 Parametric scan on toroidal and poloidal angles

For the design of the 2nd EL to be installed in EL15, a parametric scan has been performed with TORBEAM to determine the optimal poloidal and toroidal angle for each mirror. This preliminary design relies on a launcher with the same mirror configuration as EL14, except that for EL15 all mirrors will inject in the co-current direction to maximise the ECCD capabilities. For this reason, the averaged toroidal angle of the TSM (originally at $\beta \sim 18°$) is aligned to that of the BSM and MSM (which have the same toroidal launching angle $\beta \sim 25°$). Then a scan is made in β and in normalised poloidal angle γ_N (as defined in Fig. 2) to determine the optimal set of angles. For this scan, the criteria are as follows:

- The optimal value of β is chosen to maximize the ECCD (maximising the absorption is not a good criterion since 100% of absorption is reached for most of the angles of the scan).
- The optimal value of γ_N is chosen such that the overall radial range covered by EL15 is within $\rho \sim$ [0.2,0.4], to avoid a strong ECCD peak in the very centre. In addition, it is spread such that the overall ECH/ECCD profiles are smooth within $\rho \sim$ [0.2,0.4]. Fig. 7 gives an example of a scan for the TSM in the 15 MA / 5.3 T DT baseline scenario. The upper figure indicates the correspondence between γ_N and the radial location of the maximum of absorption, which is used to choose the appropriate value of γ_N for the deposition to be within $\rho \sim$ [0.2,0.4]. The middle plot allows the optimal value of β which maximises the ECCD to be selected, while the lower figure gives the ECH absorption. As previously announced, the latter is 100% (i.e. 6.7 MW for a single mirror of the EL) in most of the cases, so insufficiently selective in terms of poloidal and toroidal steering angles.

From such a scan, the optimal angles for each mirror of EL15 are chosen and summarized in Table 2. The exact radial location of each mirror has been chosen such that the ECH/ECCD profiles are smooth, as shown in Fig. 8. The study indicates that, when tuning these angles for the DT baseline scenario, the configuration is optimal also for the two half-field scenarios in L-mode

and H-mode. The configuration has been tested and proven compatible with scenarios calculated with DINA [9] for DT phases.

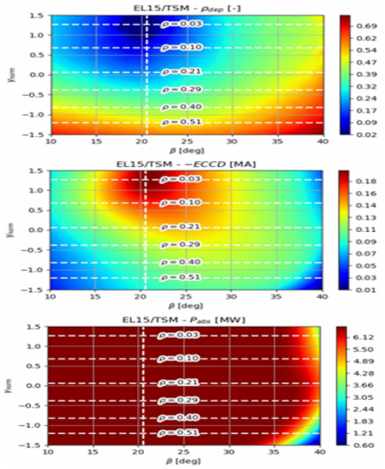

Fig. 7. Radial deposition location $\boldsymbol{\rho}$ (upper), ECCD (middle) and absorbed power (lower) for the TSM mirror for the parametric scan in the $(\boldsymbol{\beta}, \boldsymbol{\gamma_N})$ plane representing the toroidal and poloidal directions respectively, for the 134173/106 15 MA / 5.3 T DT baseline scenario.

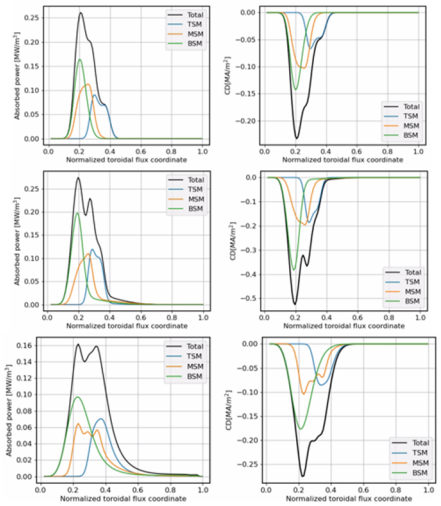

Fig. 8. ECH (left) and ECCD (right) profiles from EL15 for the DT baseline scenario (upper), the L-mode half-field scenario (middle) and the H-mode half-field scenario (lower), with the angles as defined in Table 2.

Table 2. Optimal toroidal and poloidal angles to achieve the maximum ECCD and to aim ECH/ECCD to be within the radial range ρ ~ [0.2,0.4].

Mirror	Toroidal angle β	Radial location ρ	Poloidal angle γ_N
TSM	20.5°	~ 0.3	−0.38
MSM	22°	~ 0.25	−0.49
BSM	20.5°	~ 0.2	0

4 Estimates of EC heat loads

The appropriate choice of EC operational conditions implies a minimization of EC-induced heat loads. These loads originate from shine-through losses when the plasma pressure is too low and the wave is not fully absorbed in the plasma, leading to residual beam power reaching the wall on the high field side. The other source of heat loads, as introduced in Section 2, is due to cross-polarization effects at 5.3 T inducing the presence of a fraction of X1-polarized wave, which reflects on the density cut-off layer, leading to losses on the low field side. These losses have been extensively studied and first presented in [10] for the DT baseline scenario and later in [11] for scenarios of the new baseline. The study relies on TORBEAM post-processing tools projecting the beam intensities into tangential planes at the intersection of the beam with the wall, where they form ellipses. The beam parameters are stored in the `waves` IDS such that the impact of stray radiation can be studied by reconstructing the Gaussian beams and their impact on the plasm-facing components (PFC). This approach can first be applied in vacuum, with a scan of poloidal angle for all mirrors of all launchers, as illustrated in Fig. 9 displaying the projection of the 18 ITER sectors (x-axis) associated with a projection of the wall contour in the poloidal direction (y-axis).

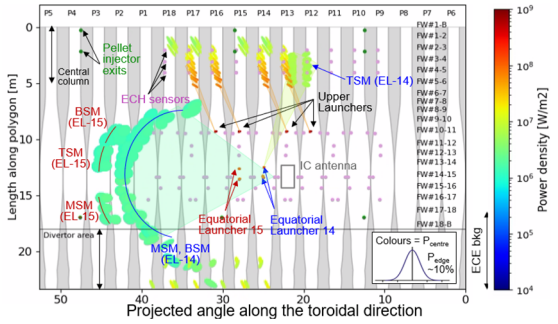

Fig. 9. Projected wall incident EC heat loads in vacuum, with a scan of poloidal angles over their full range (except for EL15 which is fixed). The entry points of beams crossing the wall contour are also explicitly displayed.

In this representation, the colour indicates the maximum power density at the centre of the ellipse, which is reduced by one order of magnitude at its edge. Such a map indicates angles which can be considered and those to avoid, to prevent damage on PFCs or specific FW panels which may undergo design simplification leading to reduced heat load tolerance. This information is essential to ensure that the FW (temporary in SRO, final in DT) is appropriate to sustain normal ECH operation.

The peak loads in Fig. 9 can appear alarming (up to many hundreds of MW/m^2), but it should be clear that they are incident loads only and will in fact be reduced by roughly a factor 100 due to the ~99% reflection coefficient of W. Of course, for injection into an empty vacuum vessel, the power will eventually be deposited on surfaces after multiple reflections, but it will be a much lower surface power density. In general, protection systems must be put in place to avoid this shine-through power deposition as much as possible. Note that the map also indicates the location of shine-through losses with plasma, since for ITER, beam bending in the plasma is quite low (of course the magnitude of shine-through losses is significantly reduced when a plasma is present). The range of the ECE background (characterising non-critical heat load level) is indicated by the vertical arrow to the left of the

colour scale of Fig. 9. It corresponds to heat loads of 100 to 200 kW/m^2, again subject to reduction by reflection.

Finally, heat loads due to cross-polarization have been studied and are shown in Fig. 10, where 5% of X1 cross-polarization has been considered. Since the level of cross-polarization is expected to be smaller, this is a conservative estimate. Fig. 10 shows the heat loads for the time range [15-215] s which covers most of the ramp-up phase and the beginning of the flat-top phase in the 15 MA / 5.3 T baseline scenario. The time traces indicate the heat load footprints going towards the entry point of the beams when the plasma density increases. For this reason the cut-off layer goes to the separatrix. Incident heat loads from the EL (UL) may reach ~20 (50) MW/m^2 but again would be reduced to the level of 0.2-0.5 MW/m^2 once reflections are taken into account. Such values are comparable to the peak stationary loads expected on the actively cooled FW due to photon and charge-exchange neutral deposition in baseline burning plasmas. They are thus perfectly manageable, but care must be taken to check that beams do not penetrate into gaps between wall elements in which case loads could be more harmful. Such gap avoidance is still under investigation (also for shine-through loads) and avoidance methods are under study.

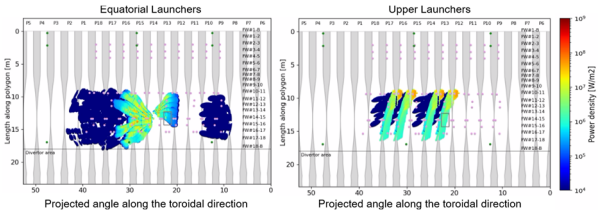

Fig. 10. Wall projected EC heat loads with plasma due to cross-polarization (5% X1 assumed), for ELs (left figure) and ULs (right figure) including a scan of poloidal angles over their full operational range (except for EL15 which has fixed angles), for the 15 MA / 5.3 T DT baseline scenario 134173/106 in the time range [15-215] s.

5 ECCD for NTM control

MHD instabilities can deteriorate the plasma confinement. They appear on rational surfaces of the safety factor profile, driven by pressure and current gradients. ECRH can reduce sawteeth taking place at the $q = 1$ rational surface [12], while ECCD can stabilise tearing modes occurring at the $q = 3/2$ and $q = 2$ surfaces [13,14,15]. A recent performance analysis [16] carried out on the UL final optical design for ITER reference scenarios indicates that the 4 ULs are needed to efficiently stabilize tearing modes for e.g. the 15 MA / 5.3 T DT baseline scenario, to inject an EC power of the order of 8-9 MW at the $q = 3/2$ with the USM and $q = 2$ rational surfaces with the LSM. The stabilization efficiency may be decreased due to the thermal deformation of the launchers, the excitation of High Order Modes and the ECCD broadening from edge density fluctuations. Using EC power modulations may hence be considered as a means to target specifically the O-point of magnetic islands, thus reducing the averaged EC power injected off-axis, which would significantly reduce the fusion gain. The best NTM control strategies for ITER are still under investigation.

6 Conclusion

The EC system is essential in ITER and next generation fusion devices to ensure robust and performant plasma operation, by providing the necessary source of heating, current drive, with the most flexible operational conditions, making it suitable to be applied in all phases of a plasma pulse. Special care should be taken in choosing the appropriate polarization and steering angle to maximise the power absorption and ensure that EC heat loads to not reach critical areas like gaps or diagnostics. ECCD is essential for NTM control to prevent islands from growing such that they lock to the wall, leading to disruptions. The best NTM control strategy for ITER is still an open question, as modelling indicates that 3-4 ULs are suitable to successfully stabilize NTMs, but strong off-axis heating may significantly reduce the fusion gain, in which case EC power modulations may be more favourable. ECH became key in the ITER new baseline to ensure core heating, thus avoiding radiative collapses, more prone to happen due to the increased W source from the wall. Yet the achievement of high fusion gain relies not only on ECH but also on ICH and NBI providing an essential source of direct ion heating, necessary to achieve the Q=10 ITER mission goal.

Acknowledgments

ITER is a Nuclear Facility INB-174. The views and opinions expressed herein do not necessarily reflect those of the ITER Organization. This publication is provided for scientific purposes only. Its contents should not be considered as commitments from the ITER organization as a nuclear operator in the frame of the licensing process. This work has been supported by the ITER Scientist Fellow Network.

References

1. A Loarte et al., The new ITER baseline, research plan and open R&D issues, Plasma Phys. Control. Fusion **67**, 065023 (2025). https://doi.org/10.1088/1361-6587/add9c9
2. T. Wauters et al., Wall conditioning by ECRH discharges and He-GDC in the limiter phase of Wendelstein 7-X, Nucl. Fusion **58**, 066013 (2018). https://doi.org/10.1088/1741-4326/aab2c9
3. R. Prater, Heating and current drive by electron cyclotron waves, Physics of Plasmas **11**, 2349 (2004). https://doi.org/10.1063/1.1690762
4. E. Poli et al., TORBEAM 2.0, a paraxial beam tracing code for electron-cyclotron beams in fusion plasmas for extended physics applications, Comp. Phys. Comm. **225**, 36 (2018). https://doi.org/10.1016/j.cpc.2017.12.018

5. F. Imbeaux et al., Design and first applications of the ITER integrated modelling & analysis suite, Nuclear Fusion **55**, 123006 (2015). https://doi.org/10.1088/0029-5515/55/12/123006
6. M. Schneider et al., Simulation of heating and current drive sources for scenarios of the ITER research plan, Nuclear Fusion **61**, 126058 (2021). https://doi.org/10.1088/1741-4326/ac34d8
7. M. Romanelli et al., JINTRAC: A System of Codes for Integrated Simulation of Tokamak Scenarios, Plasma & Fusion Research **9**, 3403023 (2014). https://doi.org/10.1585/pfr.9.3403023
8. T. Fonghetti et al., WEST L-mode record long pulses guided by predictions using Integrated Modeling, Nucl. Fusion **65**, 056018 (2025). https://doi.org/10.1088/1741-4326/adc7c7
9. R.R. Khayrutdinov and V.E. Lukash, Studies of Plasma Equilibrium and Transport in a Tokamak Fusion Device with the Inverse-Variable Technique, J. Comp. Phys. **107**, 106 (1993). https://doi.org/10.1006/jcph.1993.1211
10. J. Stober et al., Location and Quantification of non-absorbed EC-power in ITER, 49th European Conference on Plasma Physics, Bordeaux, France (2023). https://lac913.epfl.ch/epsppd2/2023/html/Th/Th_MCF61_Stober.pdf
11. M. Schneider et al., IMAS modelling of First Wall EC heat loads for the ITER rebaseline, EPJ Web of Conferences **313**, 01004 (2024). https://doi.org/10.1051/epjconf/202431301004
12. I. Chapman et al., Power requirements for electron cyclotron current drive and ion cyclotron resonance heating for sawtooth control in ITER, Nucl. Fusion **53**, 066001 (2013). https://doi.org/10.1088/0029-5515/53/6/066001
13. P. H. Rutherford, Nonlinear growth of the tearing mode, Phys. Fluids **16** 1903 (1973). https://doi.org/10.1063/1.1694232
14. O. Sauter. et al., Marginal β-limit for neoclassical tearing modes in JET H-mode discharges, Plasma Phys. Control. Fusion **44**, 1999 (2002). https://doi.org/10.1088/0741-3335/44/9/315
15. M. Maraschek, Control of neoclassical tearing modes, Nucl. Fusion **52**, 074007 (2012). https://doi.org/10.1088/0029-5515/52/7/074007
16. L. Figini, 2025, to be published